ENCIT 2002

IX CONGRESSO BRASILEIRO DE ENGENHARIA E CIÊNCIAS TÉRMICAS

9th BRAZILIAN CONGRESS OF THERMAL ENGINEERING AND SCIENCES

ABCM

Paper CIT02-0602

FREE SURFACE FLOWS OF OLDROYD-B LIQUIDS IN ROLL COATING PROCESS

Gladys A. Zevallos
gzevallo@mec.puc-rio.br

Marcio da Silveira Carvalho
Departament of Mechanical Engineering, Pontifícia Universidade Católica do Rio de Janeiro.
Rua Marquês de São Vicente, 225. Gávea, Rio de Janeiro, 22453-900, Brazil.
msc@mec.puc-rio.br

Matteo Pasqualli
Departament of Chemical Engineering, Rice University.
6100 Main St., Houston, TX, 77005, USA.
mp@rice.edu

Abstract.

Roll coating is distinguished by the use of one or more gaps between rotating cylinders to meter and apply a liquid layer to a substrate. Except at low speeds, the film-splitting flow that occurs in forward roll coating is three-dimensional and results in more or less regular stripes in the machine direction. This instability can limit the speed of the process if a smooth film is required as a final product. For Newtonian liquids the stability of the film-split flow is determined by the competition of capillary and viscous forces: a critical value of the ratio between these two forces, i.e. the Capillary Number, marks the onset of meniscus nonuniformity. Non-Newtonian behavior can drastically change the conditions at the onset of the instability and the resulting three-dimensional flow. At extreme conditions the ribs may grow and form filaments that eventually break in such a way as to form small drops, a phenomenon known as spatter or misting. Misting is a serious problem in many industrial application and it limits the speed of many processes. However, the mechanisms by which rheological properties of the liquid act are still a matter of research. In this work, the steady two dimensional film-split flow of viscoelastic liquids is analyzed by solving the conservation equations with a differential constitutive model, Oldroyld-B equation, to describe the mechanical behavior of the flowing liquid. The presence of the free surface and the differential constitutive model makes this problem extremely complex. The equations are solved by the Finite Element Method and Newton's method.

Keywords: *roll coating, free surface flow, Oldroyld-B model, finite element method*

1. Introduction

Roll coating is widely used to apply a thin liquid layer to a continuous, flexible substrate. Except at low speeds, the flow is three-dimensional and results in more or less regular stripes in the machine direction, as sketched in Fig.(1). This type of instability, or rather the three-dimensional flow to which it may lead, is commonly called *ribbing*. It can limit the speed of the process if a smooth film is required as a final product. The flow and the instability of the splitting of a Newtonian liquid as it exits from between two rotating rolls has been extensively studied (see Pearson, 1960; Pitts and Greiller, 1961; Mill and South, 1967; J. Greener and Middleman, 1980; H. Benkreira and Wilkinson, 1982; and D. J. Coyle and Scriven, 1990). The stability of the flow is determined by the competition of capillary and viscous forces near the free surface. A critical value of the ratio between these two forces, i.e. the Capillary number $Ca \equiv \mu V/\sigma$, marks the onset of the free surface nonuniformity. Here, μ is the liquid viscosity, σ its surface tension and V is the mean roll speed.

In practice, coating solutions often contain polymers. Non-Newtonian behavior can drastically change the nature of the flow near the free surface and consequently alter the performance of a coater. The first analyses of non-Newtonian effects in roll coating flows were restricted to shear-thinning behavior and simple power-law models. J. Greener and Middleman, 1980, demonstrated that a shear-thinning liquid is always more stable than a Newtonian liquid when the basis of comparison is equal viscosities at a nominal gap shear rate of $\dot{\gamma} = V/H_0$, where H_0 is half the gap between the rolls. T. Bauman and Middleman, 1982, experimentally tested the effect of certain polymer additives on the ribbing instability. They observed that the critical speed at which ribbing first appeared was smaller than in the case of a Newtonian liquid. They advanced simple arguments about the effect of liquid elasticity on the stability of the flow, and concluded that first normal stress difference destabilizes the flow. The formation of small liquid drops at the film split meniscus, a phenomenon known as

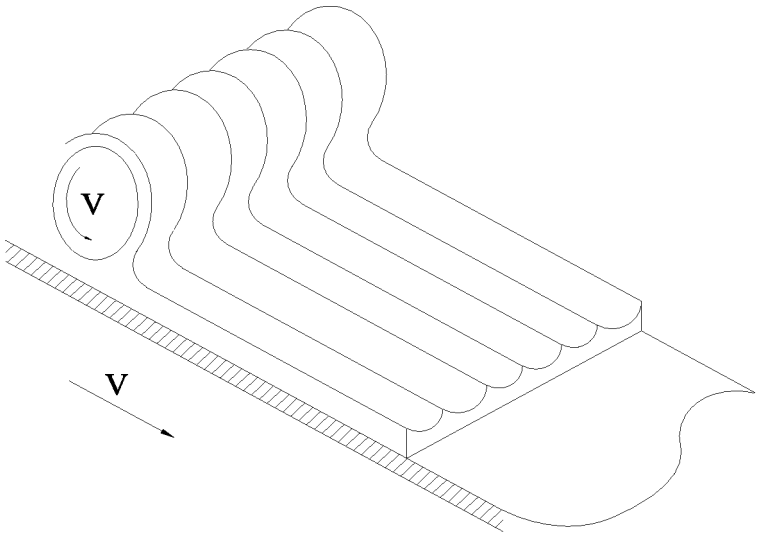

Figure 1: Sketch of ribbing instability in forward roll coating.

spatter and misting, was studied by Glass, 1978. He observed roll spatter in coating of aqueous dispersions of colloidal polymer plus other ingredients in 'latex' paints by evaluating several trade paints and comparing their propensity to spatter. The main conclusion was that paints with high apparent extensional viscosity produced extremely large and stable filaments. Glass, 1988, addressed the spattering phenomenon in commercial paints. They found that the greater the apparent extensional viscosity, as measured by the fiber-suction technique, the longer the filament in their experiments and greater the misting in certain applications. M. S. Carvalho and Scriven, 1995, and latter P. Dontula and Scriven, 1996, analyzed experimentally the film splitting flow of aqueous solution of PEG and PEO. They concluded that when minute amounts of flexible polymer are present, the onset of the three-dimensional instability occurs at much lower speeds than in the Newtonian case.

Accurate theoretical predictions of the onset of ribbing when viscoelastic liquids are used is still not available. The mechanisms by which the liquid elasticity makes the flow unstable at Capillary numbers much lower than in the Newtonian case is not understood. In order to model any flow instability, it is crucial to develop accurate theoretical analysis of both the base flow, in this case steady and two-dimensional, and the response of that flow to all physically admissible infinitesimal disturbances.

Coating flow modelling of non-Newtonian liquids must rely on theories that can account for the different behavior of microstructured liquids in shear and extensional flow. Moreover, coating flows always involve free surface. The domain where the differential equations are posed is unknown *a priori* and it is part of the solution. These two characteristics makes the problem extremely complex and they are the main reason why complete two dimensional solution of viscoelastic free surface flows is rare.

In this work, the two-dimensional, viscoelastic flow near the film split meniscus of a forward roll coating gap is analyzed by solving with the Finite Element method the momentum and continuity equations coupled with the Oldroyd-B differential constitutive model. The results show how the liquid properties affect the stress field and reveal a new elastic mechanism that may explain the early onset of the three-dimensional instability when viscoelastic liquids are used.

2. Theoretical Model

The flow domain where the governing equations are integrated is sketched in Fig.(2). The two rolls are moving from left to right in the figure at equal speed V. The minimum clearance between the rolls is $2H_0$. The position of the meniscus is unknown *a priori* and it is a function of the liquid properties and operating conditions.

2.1. Conservation equations

For incompressible and isothermal flow, the momentum and continuity equations are:

$$\rho \underline{v} \cdot \nabla \underline{v} - \nabla \cdot \underline{\underline{T}} = \underline{0} \tag{1}$$

$$\nabla \cdot \underline{v} = 0 \tag{2}$$

where ρ is the liquid density and $\underline{\underline{T}} \equiv -p\underline{\underline{I}} + \underline{\underline{\tau}} + \underline{\underline{\sigma}}$ is the total stress tensor, the sum of pressure p, viscous $\underline{\underline{\tau}}$ and elastic stress $\underline{\underline{\sigma}}$.

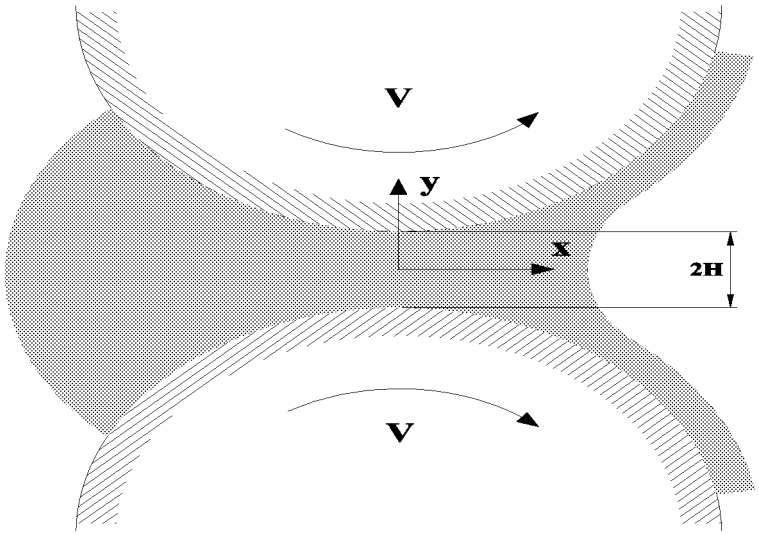

Figure 2: Flow domain with free surface.

The boundary conditions are:

1. *Inflow: Flooded condition.*

$$p = P_0 \tag{3}$$

Here P_0 is set to zero.

2. *Roll surfaces: No-slip, no-penetration.*

$$\underline{v} = \Omega R \underline{t} = V \underline{t} \tag{4}$$

R is the roll radius, Ω is the angular speed of the rolls, and $\underline{t}$ is the unit tangent vector to the roll surface in the direction of rotation.

3. *Free surface: Force balance and kinematic condition.*

$$\underline{n} \cdot \underline{\underline{T}} = \sigma \frac{d\underline{t}}{ds} - \underline{n} P_{amb} \quad \text{and} \quad \underline{n} \cdot \underline{v} = 0 \tag{5}$$

σ is the liquid surface tension, s is the coordinate along the free surface, and P_{amb} is the ambient pressure. It is set to zero.

4. *Outflow: Fully developed flow.*

$$\underline{n} \cdot \nabla \underline{v} = 0 \tag{6}$$

In order to solve the differential equations, the stress tensor $\underline{\underline{T}}$ has to be related to the local rate of deformation of the liquid. The constitutive model used here is discussed in the following subsection.

2.2. Constitutive model

Microstructured materials, such as polymeric solutions, behave differently in shear and extensional flows. The length, stiffness and branchiness of polymer molecules strongly affect the shear and elongational response of the solution. Here the mechanical behavior of the viscoelastic liquid is modelled by the *coarse-grained* theory presented by Pasquali, 2000. Coarse-grained theories introduce field variables that are expectation values of microstructural features, and equations of change that describe how these features evolve and how they interact with the flow.

The salient microstructural features of a flowing polymer are the stretch and orientation of the polymer chains. These can be represented by the conformation tensor $\underline{\underline{M}}$. The transport equation of $\underline{\underline{M}}$ is

$$\underline{v} \cdot \nabla \underline{\underline{M}} - 2\xi \frac{\underline{\underline{D}} : \underline{\underline{M}}}{\underline{\underline{I}} : \underline{\underline{M}}} \underline{\underline{M}} - \zeta(\underline{\underline{M}} \cdot \underline{\underline{D}} + \underline{\underline{D}} \cdot \underline{\underline{M}} - 2\frac{\underline{\underline{D}} : \underline{\underline{M}}}{\underline{\underline{I}} : \underline{\underline{M}}} \underline{\underline{M}}) - \underline{\underline{M}} \cdot \underline{\underline{W}} - \underline{\underline{W}}^T \cdot \underline{\underline{M}} + \frac{1}{\lambda}(g_0 \underline{\underline{I}} + g_1 \underline{\underline{M}} + g_2 \underline{\underline{M}}^2) = 0 \tag{7}$$

where $\underline{\underline{D}}$ is the rate of strain tensor, $\underline{\underline{W}}$ is the vorticity tensor, λ is the characteristic relaxation time of the polymer, $\xi(\underline{\underline{M}})$ and $\zeta(\underline{\underline{M}})$ represent the resistance to stretching and relative rotation of polymer segments, and $g_0(\underline{\underline{M}})$, $g_1(\underline{\underline{M}})$ and $g_2(\underline{\underline{M}})$ define the rate of relaxation of the polymer segments. Pasquali, 2000, presents a complete description of each term of Eq.(7).

As mentioned before, the total stress tensor $\underline{\underline{T}}$ is split into isotropic, viscous and elastic components:

$$\underline{\underline{T}} = -p\underline{\underline{I}} + \underline{\underline{\tau}} + \underline{\underline{\sigma}}. \tag{8}$$

The viscous stress obeys Newton's law of viscosity,

$$\underline{\underline{\tau}} = 2\mu\underline{\underline{D}}, \tag{9}$$

and the elastic stress is a function of the conformation tensor:

$$\underline{\underline{\sigma}} = 2\rho(\xi - \zeta)\frac{\underline{\underline{M}}}{\underline{\underline{I}} : \underline{\underline{M}}}\underline{\underline{M}} : \frac{\partial a}{\partial \underline{\underline{M}}} + 2\rho\zeta\underline{\underline{M}} \cdot \frac{\partial a}{\partial \underline{\underline{M}}}, \tag{10}$$

where $a(T, \underline{\underline{M}})$ is the specific free energy.

In the particular case of Oldroyd-B model, $\xi = \zeta = 1$, $g_0 = -1$, $g_1 = 1$, $g_2 = 0$, and $a = G/(2\rho)tr(\underline{\underline{M}})$. In order to make the elastic stress traceless, the equation for the conformation tensor is modified accordingly. The constitutive relation becomes:

$$\underline{v} \cdot \nabla\underline{\underline{M}} - (\underline{\underline{M}} \cdot \underline{\underline{D}} + \underline{\underline{D}} \cdot \underline{\underline{M}}) - (\underline{\underline{M}} \cdot \underline{\underline{W}} + \underline{\underline{W}}^T \cdot \underline{\underline{M}}) + \frac{1}{\lambda}(-\underline{\underline{I}} + \underline{\underline{M}} - \frac{1}{3}tr(\underline{\underline{M}})\underline{\underline{I}}) = 0 \tag{11}$$

$$\underline{\underline{\sigma}} = G\underline{\underline{M}} \tag{12}$$

The parameters of the constitutive model are: the solvent viscosity μ, the polymer elastic modulus G, and the relaxation time λ. The polymer viscosity η_p is a function of the polymer elastic modulus and the relaxation time, $\eta_p = G\lambda$.

3. Solution Method

Because of the free surfaces, the flow domain at each parameter is unknown *a priori*. In order to solve this free boundary problem by means of standard techniques for boundary value problems, the set of differential equations and boundary conditions posed in the unknown domain has to be transformed to an equivalent set defined in a known reference domain. Detailed description of methods to solve free boundary problems are presented by Kistler and Scriven, 1983, Christodoulou and Scriven, 1990, and Carvalho and Scriven, 1997. A brief description of the method used is presented. The transformation of the equation set is made by a mapping $\underline{x} = \underline{x}(\underline{\xi})$ that connects the two domains. The unknown physical domain is parameterized by the position vector $\underline{x}$, and the reference domain by $\underline{\xi}$. The mapping used here is the one presented by de Santos, 1991. He showed that a functional of weighted smoothness can be used successfully to construct the sorts of maps involved here. The inverse of the mapping that minimizes the functional is governed by an elliptic differential equation identical with the one encountered in diffusional transport with variable diffusion coefficients. The coordinates $\underline{\xi}$ of the reference domain satisfy

$$\nabla \cdot (\underline{\underline{\tilde{D}}}\underline{\xi}) = 0 \tag{13}$$

$\underline{\underline{\tilde{D}}}$ is the tensor of diffusion-like coefficients used to control element spacing. Boundary conditions are needed in order to solve the second-order partial differential equations Eq.(13). Along solid walls and synthetic inlet and outlet plates, the boundary is located by imposing a relation between the coordinates from the equation that describes the shape of the boundary, and stretching functions are used to distribute the points along the boundaries. The free boundary (gas-liquid interface) is located by imposing the kinematic condition Eq.(5). The discrete version of the mapping equation Eq.(13) is generally referred to as mesh generation equation. It describes the inverse mapping $\underline{\xi} = \underline{\xi}(\underline{x})$. To evaluate $\underline{x} = \underline{x}(\underline{\xi})$, the diffusion equation that describe the mapping also has to be transformed to the reference configuration.

Computational methods to solve viscoelastic flows are still an active area of research. The method used here is the modification on the DAVSS-G/SUPG finite element method (M. J. Szady and Brown, 1995, and J. Sun and Brown, 1999) presented by Pasquali, 2000.

In order to have a continuous representation of the velocity gradient field, an additional variable $\underline{\underline{L}}$, called the interpolated velocity gradient, is introduced:

$$\underline{\underline{L}} - \nabla\underline{v} + \frac{1}{tr\underline{\underline{I}}}(\nabla \cdot \underline{v})\underline{\underline{I}} = 0 \tag{14}$$

The weighted residual form of all the governing equations is

$$\underline{r}^{x,\alpha} = \int_{\Gamma_0} \psi_x^\alpha \underline{n} \cdot \underline{\underline{\tilde{D}}} \cdot \nabla \underline{\xi} d\Gamma_0 - \int_{\Omega_0} \nabla \psi_x^\alpha \cdot \underline{\underline{\tilde{D}}} \cdot \nabla \underline{\xi} f d\Omega_0 \tag{15}$$

$$r^{c,\alpha} = \int_{\Omega_0} \psi_c^\alpha \nabla \cdot \underline{v} f d\Omega_0 \tag{16}$$

$$\underline{r}^{m,\alpha} = \int_{\Omega_0} \psi_m^\alpha (\rho \underline{v} \cdot \nabla \underline{v}) f d\Omega_0 - \int_{\Omega_0} \psi_x^\alpha \nabla \cdot \underline{\underline{T}} f d\Omega_0 - \int_{\Gamma_0} \psi_m^\alpha \underline{n} \cdot \underline{\underline{T}} d\Gamma_0 \tag{17}$$

$$\underline{\underline{R}}^{L,\alpha} = \int_{\Omega_0} \psi_L^\alpha \left(\underline{\underline{L}} - \nabla \underline{v} + \frac{1}{tr \underline{\underline{I}}} (\nabla \cdot \underline{v}) \underline{\underline{I}} \right) f d\Omega_0 \tag{18}$$

$$\underline{\underline{R}}^{M,\alpha} = \int_{\Omega_0} \psi_M^\alpha \left(\underline{v} \cdot \nabla \underline{\underline{M}} - (\underline{\underline{M}} \cdot \underline{\underline{D}} + \underline{\underline{D}} \cdot \underline{\underline{M}}) - (\underline{\underline{M}} \cdot \underline{\underline{W}} + \underline{\underline{W}}^T \cdot \underline{\underline{M}}) + \frac{1}{\lambda} (-\underline{\underline{I}} + \underline{\underline{M}} - \frac{1}{3} tr(\underline{\underline{M}}) \underline{\underline{I}}) \right) f d\Omega_0 \tag{19}$$

The first subscript on the residuals identifies the type of residual equation (mesh, continuity, momentum, interpolated gradient, or conformation). The second (Greek) subscript labels the residual equation in the set. Each variable is approximated with a finite combination of basis functions:

$$\underline{x} \equiv \underline{X}^\beta \varphi_{\mathbf{x}}^\beta \quad ; \qquad p \equiv P^\beta \varphi_p^\beta \quad ; \qquad \underline{v} \equiv \underline{V}^\beta \varphi_{\mathbf{v}}^\beta \quad ; \qquad \underline{\underline{L}} \equiv \underline{\underline{L}}^\beta \varphi_{\mathbf{L}}^\beta \quad ; \qquad \underline{\underline{M}} \equiv \underline{\underline{M}}^\beta \varphi_{\mathbf{M}}^\beta \tag{20}$$

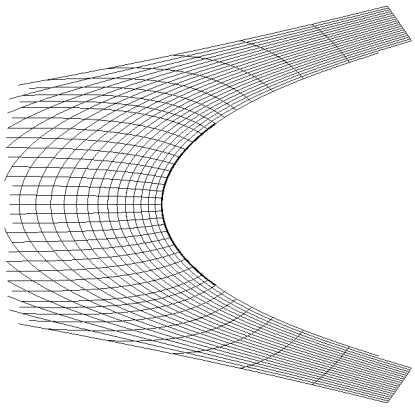

Figure 3: Detail of mesh near free surface.

Lagrangian biquadratic basis functions are used for position and velocity, linear discontinuous for pressure, and Lagrangian bilinear for interpolated velocity gradient and conformation. The mesh generation equations and the momentum equation are weighted with Lagrangian biquadratic basis functions (Galerkin), the continuity equation with linear discontinuous (Galerkin), and the velocity gradient interpolation with Lagrangian bilinear (Galerkin). The conformation transport equation is weighted with the Streamline-Upwind Petrov-Galerkin method, $\psi_{\mathbf{M}} \equiv \varphi_{\mathbf{M}} + h^u \mathbf{v} \cdot \nabla \varphi_{\mathbf{M}}$. The upwind parameter h^u coincides with the characteristic size of the smallest element in the finite element mesh.

The set of nonlinear algebraic equations that arises from applying the method of weighted residuals and the variables representation in terms of basis functions is solved by Newton's method with analytical Jacobian and first order arclength continuation. Detail of the mesh near the free surface is shown in Fig.(3). The domain was divided into 1760 elements and the total number of degrees of freedom of the problem was 49260.

4. Results

The important dimensionless parameters for this situation are:

1. Reynolds number: $Re = \rho V R / H_0$
2. Capillary number: $Ca = \mu V / \sigma$

3. Dimensionless gap: H_0/R
4. Weissember number: $We = \lambda V/H_0$
5. Solvent to total viscosity ratio: $\beta = \mu/\mu + \eta_p$

The predictions presented here are for vanishing Reynolds number and fixed dimensionless gap $H_0/R = 0.01$.

4.1. Newtonian Liquids

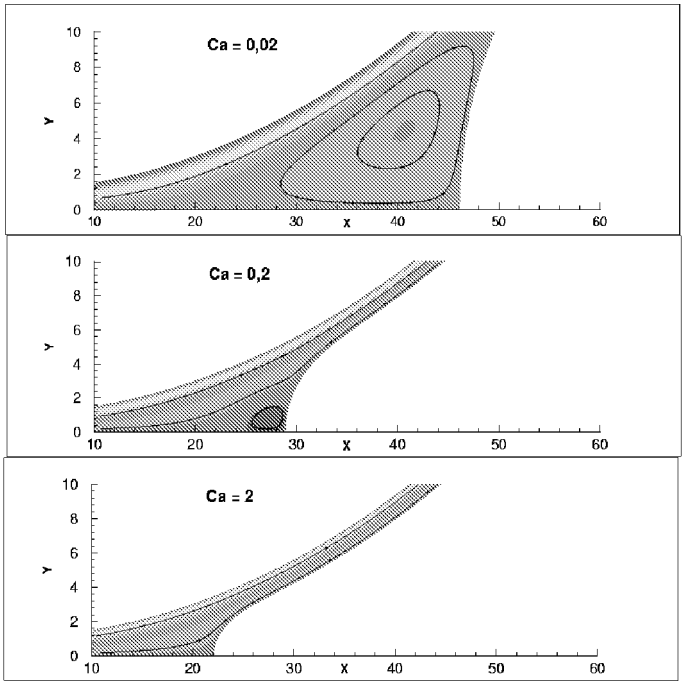

Figure 4: Streamlines near the free surface: (a) $Ca = 0.02$, (b) $Ca = 0.2$, and (c) $Ca = 2$.

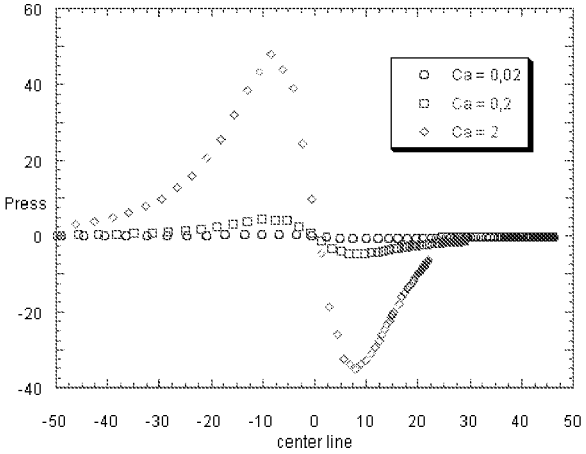

Figure 5: Pressure distribution along the centerline for different capillary numbers.

The film-splitting flow is strongly affected by capillary number. If surface tension is strong compared to the viscous forces, i.e. at low capillary numbers, the meniscus is pulled away from the gap and a large recirculation attached to the free surface is formed. As the capillary number rises, the meniscus recedes and the recirculation disappears, as shown in Fig.(4). Because the rolls are rotating at equal speed, the flow is symmetric and only half of the flow domain is presented. At $Ca = 2$, there is only one stagnation point at the free surface, located at the mid-plane between the rolls.

The pressure peak in the converging part of the gap and its valley in the diverging part become more pronounced as the rolls rotate faster, i.e. as capillary number rises, as shown in Fig.(5). The pressure distribution curves terminate at the film split, where the subambient pressure is due to the capillary pressure jump at the curved interface. The jump is greater the higher the capillary number because the meniscus is more sharply curved. Capillary number also has a strong effect on the pressure gradient at the meniscus. Because the instability that leads to a wavy free surface in the transverse direction is driven by this adverse pressure gradient, the likelihood of ribbing rises with capillary number. Therefore, at a given gap H_0/R, there is a critical capillary number above which the flow is unstable and ribbing occurs.

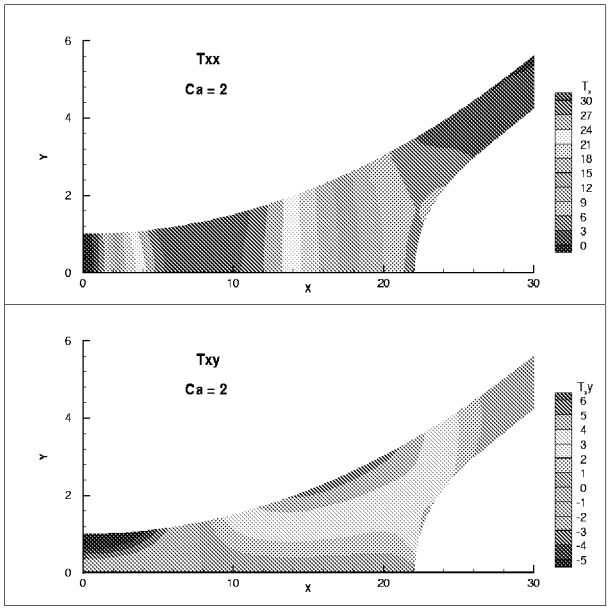

Figure 6: Stress field in the case of Newtonian liquid. $Ca = 2$.

The stress field near the free surface at $Ca = 2$ is shown in Fig.(6). The shear stress T_{xy} is strong near the minimum gap and close to the roll surface in the region where the fluid is accelerated. The normal component T_{xx} of the stress field is maximum between the rolls at $x \approx 8$. Downstream of this point, the stress falls as the liquid has to decelerate to zero velocity at the stagnation point.

4.2. Viscoelastic Liquids

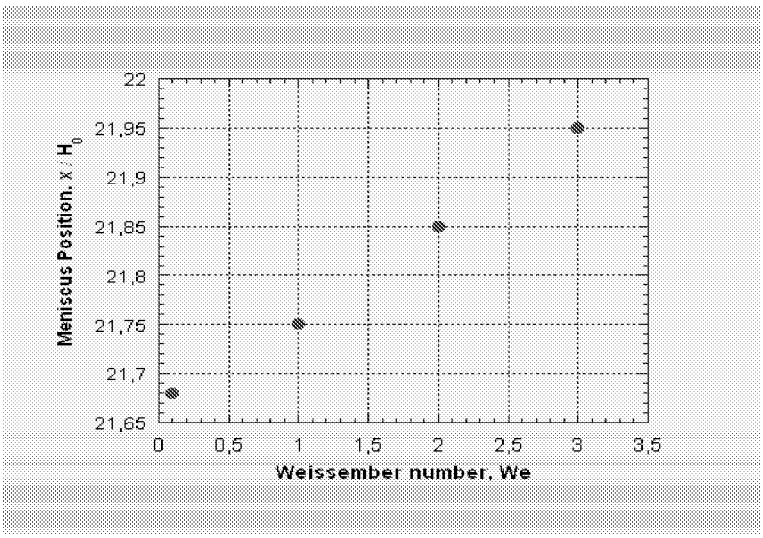

Figure 7: Meniscus position as a function of Weisember number.

The flow of a viscoelastic liquid near the film split meniscus of a forward roll coater, modelled by the Oldroyld-B equation, was computed at solvent to total viscosity ratio $\beta = 0.59$.

The elasticity of the liquid, represented by the Weisemberg number We pushes the meniscus away from the gap, as illustrated in Fig.(7). However, in the range of Weisember number explored, this change in the flow is weak and cannot explain the observed early onset of ribbing when viscoelastic liquids are used.

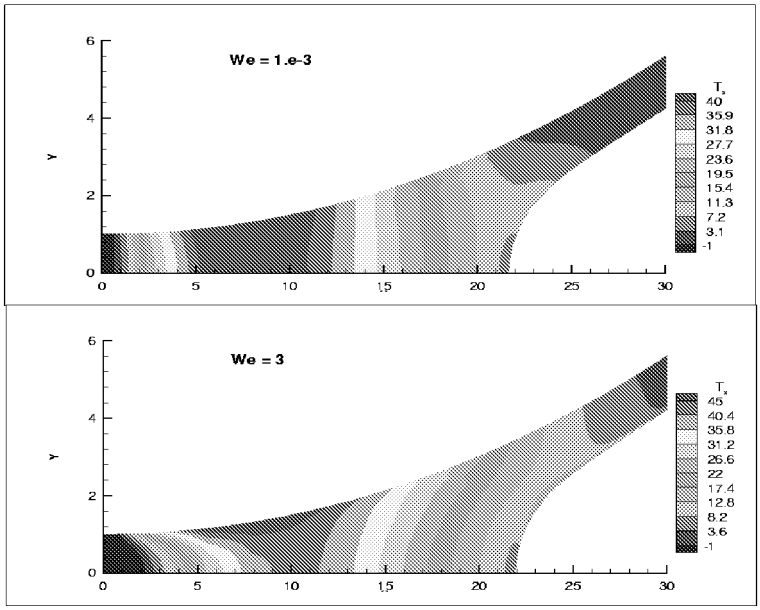

Figure 8: Evolution of the stress component T_{xx} with the liquid elasticity. (a) $We = 19^{-3}$; (b) $We = 3$.

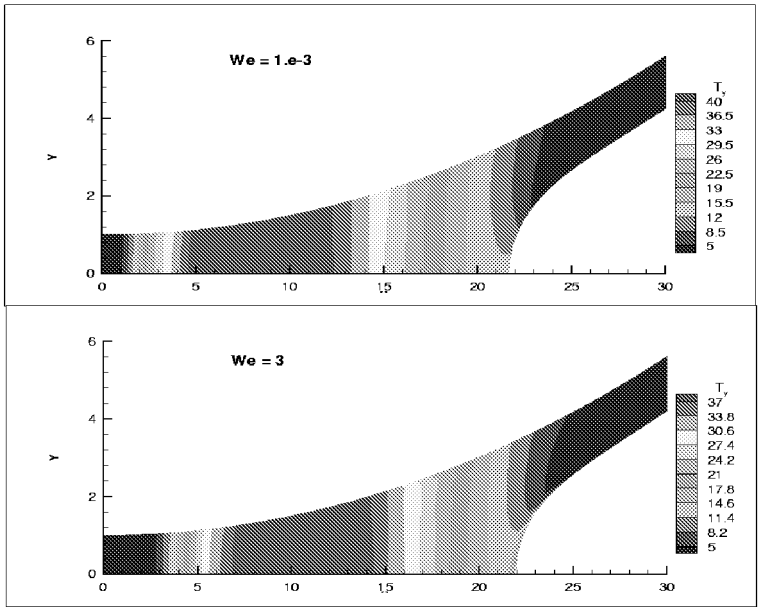

Figure 9: Evolution of the stress component T_{yy} with the liquid elasticity. (a) $We = 19^{-3}$; (b) $We = 3$.

The total stress field evolution as a function of the Weisember number at $Ca = 2$ is shown in Figs.(8) and (9). At low We, the behavior is similar to the Newtonian case, as expected. As the elasticity of the liquid becomes stronger, the region of maximum stress is shifted downstream, the gradient along the centerline of the stress component T_{xx} rises and an elastic stress boundary layer appears attached to the free surface in the region where the acceleration of the liquid is high. Near the stagnation point, an elastic stress component T_{yy} boundary layer is also formed at high Wesemberg number. The high stresses inside boundary layers change the force balance at the meniscus and may alter the critical capillary number at the onset of ribbing.

The liquid elasticity also creates compressive elastic forces in the transverse direction. Figure (10) shows the field of the normal transverse component of the elastic part of the stress tensor σ_{zz} at $Ca = 2$, $We = 10^{-3}$ and $We = 3$. At low Weisember number, the transverse stress component is negligible, as expected. As Weisember number rises, compressive transverse elastic stress appears. Near the film-split free surface, a stress

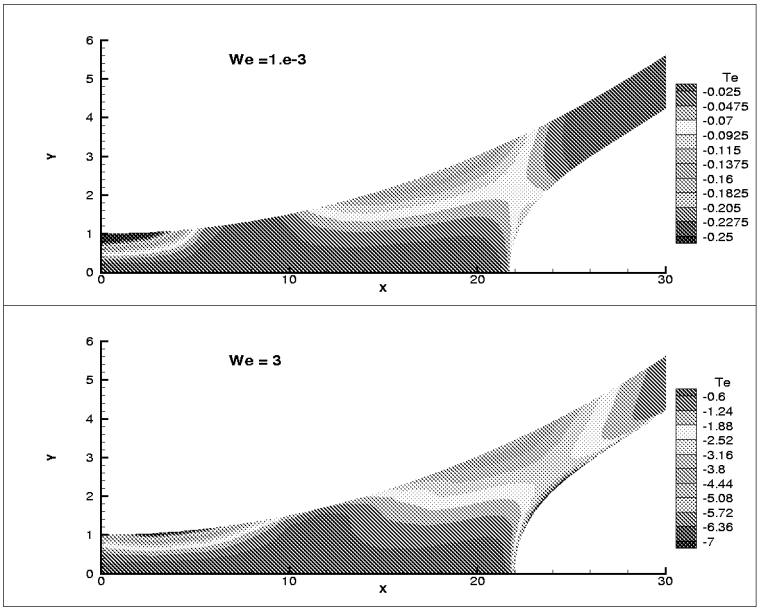

Figure 10: Transverse component of the normal elastic stress as a function of Weisember number.

boundary layer is formed and the compressive stress there is high. Figure (11) shows a zoom of σ_{zz} near the free surface. The compressive force destabilize the flow with respect to transverse disturbance causing the free surface to buckle. This force is not present in the case of Newtonian liquids. This new elastic mechanism may be responsible for the early onset of ribbing in roll coating of elastic liquids.

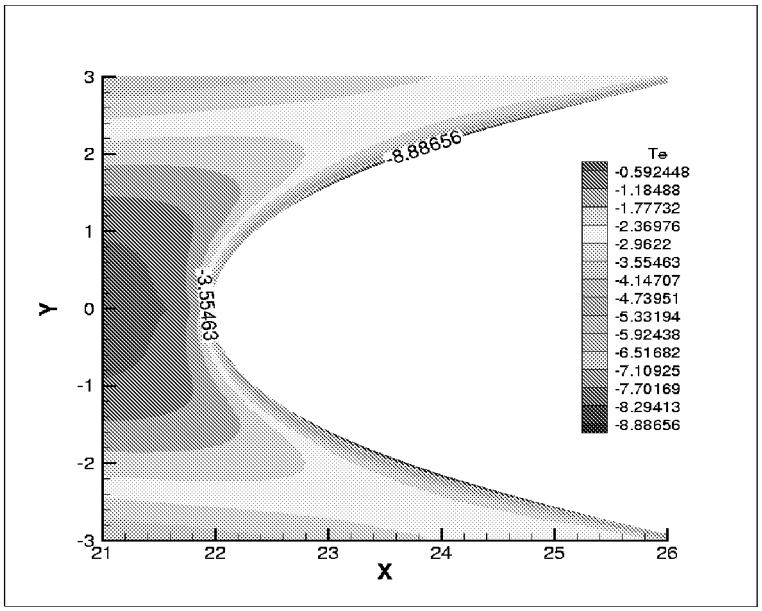

Figure 11: Detail of elastic compressive stress boundary layer near the film split meniscus.

5. Final Comments

Polymer additives in coating liquids alter their performance in the coating gap. In the specific case of forward roll coating, experiments have shown that when minute amounts of flexible polymer are present, the onset of three-dimensional instability occurs at much lower speeds than in the Newtonian case. The mechanisms by which the liquid elasticity makes the flow unstable is not completely understood and it is studied here.

The two-dimensional flow in a forward roll coating bead of viscoelastic liquids was analyzed by solving the continuity and momentum equations coupled with the Oldroyld-B differential constitutive model. The system of partial differential equations was solved with the Finite Element Method. The results reveal the appearance of elastic stress boundary layers near the free surface and compressive elastic stress at the film split meniscus

that tend to destabilize the free surface with respect to three-dimensional instability. This new mechanism may explain the early onset of ribbing observed when viscoelastic liquids are used.

6. Acknowledgments

Gladys Zevallos was supported with a scholarship from CAPES. This work was funded by grants from CNPq and FAPERJ.

7. References

Carvalho, M. S. and Scriven, L. E., 1997, Flows in forward deformable roll coating gaps: comparision between spring and plane-strain models of roll cover., "J. Comp. of Phys.", Vol. 138, pp. 449–479.

Christodoulou, K. N. and Scriven, L. E., 1990, Discretization of free surface flows and other moving boundary problems., "J. Comp. of Phys.", Vol. 99, pp. 39–55.

D. J. Coyle, C. W. M. and Scriven, L. E., 1990, Stability of symmetric film-splitting between counter-rotating cylinders., "Journal of Fluid Mechanics", Vol. 216, pp. 437.

de Santos, J. M., 1991, "Two-phase cocurrent downflow through constricted passages.", PhD thesis, University of Minnesota, Minneapolis, MN.

Glass, J. E., 1978, Dynamics of roll spatter and tracking: PartI. Commercial latex trade paints, "J. Coating Tech.", Vol. 640, pp. 53.

Glass, J. E., 1988, Dynamic uniaxial extensional viscosity of polymer(DUEV): effects in roll applications II. Polymer blend studies, "J. Rheol.", Vol. 32, pp. 199.

H. Benkreira, M. F. E. and Wilkinson, W. L., 1982, Ribbing instability inthe roll coating of Newtonian fluids., "Plastics and Rubber Processing and Aplications", Vol. 2, pp. 137.

J. Greener, T. Sullivan, B. T. and Middleman, S., 1980, Ribbing instability of a two-roll coater: Newtonian fluids., "Chem. Eng. Commum.", Vol. 5, pp. 73.

J. Sun, M. D. Smith, R. C. A. and Brown, R. A., 1999, Finite element method for viscoelastic flows based on the discrete adaptative viscoelastic stress splitting and the discontinuous galerking method: DAVSS-G/DG., "J. Non-Newtonian Fluid Mech.", Vol. 86, pp. 281–307.

Kistler, S. F. and Scriven, L. E., 1983, Coating flows., "Computational Analysis of Polymer Processing", Vol. 138, pp. 243.

M. J. Szady, T. R. Salamon, A. W. L. R. C. A. and Brown, R. A., 1995, Flows in forward deformable roll coating gaps: comparision between spring and plane-strain models of roll cover., "J. Non-Newtonian Fluid Mech.", Vol. 59, pp. 215–243.

M. S. Carvalho, P. D. and Scriven, L. E., 1995, Non-Newtonian Effects on the Ribbing Instability., "Proceedings of the TAPPI Coating Conference", Vol. 1, Dallas, TX, USA.

Mill, C. C. and South, G. R., 1967, Formation of ribs on rotating rollers., "Journal of Fluid Mechanics", Vol. 28, pp. 523.

P. Dontula, M. Pasquali, C. W. M. and Scriven, L. E., 1996, Viscoelastic Effects in forward roll coating., "Proceedings of the XIIth International Congress on Rheology", Vol. 1, Montreal, Canada.

Pasquali, M., 2000, "Polymer molecules in free surface flows.", PhD thesis, University of Minnesota, Minneapolis, MN.

Pearson, J. R. A., 1960, The stability of uniform viscous flow under rollers and spreaders., "Journal of Fluid Mechanics", Vol. 7, pp. 481.

Pitts, E. and Greiller, J., 1961, The flow of thin liquid films between rollers., "Journal of Fluid Mechanics", Vol. 11, pp. 33.

T. Bauman, T. S. and Middleman, S., 1982, Ribbing instability in coating flows: Effect of polymer additives., "Chem. Eng. Commum.", Vol. 14, pp. 35.